CHIN. PHYS. LETT. Vol. 37, No. 8 (2020) 088501

Polymer-Decorated 2D MoS_2 Synaptic Transistors for Biological Bipolar Metaplasticities Emulation

Yuhang Zhao(赵宇航), Biao Liu(刘标), Junliang Yang(阳军亮), Jun He(何军)*, and Jie Jiang(蒋杰)*

Hunan Key Laboratory of Super Microstructure and Ultrafast Process, School of Physics and Electronics, Central South University, Changsha 410083, China

(Received 17 May 2020; accepted 12 June 2020; published online 28 July 2020)

Biological bipolar metaplasticities were successfully mimicked in two-dimensional (2D) MoS_2 transistors via the implementation of two different MoS_2 surface decorations, poly (vinyl alcohol) (PVA) and chitosan bio-polymers. Interestingly, the depressing metaplasticity was successfully mimicked when the PVA bio-polymer was used as the surface decoration layer, whereas the metaplasticity of long-term potentiation was realized when the chitosan bio-polymer was taken as the surface decoration layer. Furthermore, the electronic band structures of the 2D MoS_2 devices with different surface decorations were further investigated using first-principles calculations for understanding the underlying mechanisms of such bipolar metaplasticities. These results will deepen our understanding of metaplasticity, and have great potential in neuromorphic computing applications.

PACS: 85.30.Tv, 85.30.−z, 85.35.−p DOI: 10.1088/0256-307X/37/8/088501

Synaptic strength (weight), in the human brain, can be regulated by ionic species and concentrations precisely.[1,2] This phenomenon in neuroscience is considered as the synaptic plasticity, which plays an important role in memory and learning. Specifically, the long-term depression (LTD, i.e., weakening of the connection between neurons) and long-term potentiation (LTP, i.e., strengthening of the connection between neurons) are two different key characteristics of synaptic plasticity observed in CA1 (region of the hippocampus).[3]

Most interestingly, synaptic plasticity itself can be dynamically modulated by historical activity in biological systems, which is often regarded to be metaplasticity.[4] Different from the normal synaptic plasticity, this primary feature highlights a prior stimulus that does not cause obvious changes in synaptic transmission, but rather changes the duration or magnitude of subsequent synaptic plasticity.[4,5] Dynamically linked the previous neural activity with the current response, metaplasticity is a particularly fascinating regulatory mechanism in terms of adaptive behaviors (memory and learning) and maladaptive behaviors, such as post-traumatic stress disorder and phobias.[6] Therefore, metaplasticity is thought to be a higher-order form of synaptic plasticity which can also be called "plasticity of synaptic plasticity".[7] In general, unipolar metaplasticity exists in two main effects: either (i) facilitate subsequent LTP through activating group 1 metabotropic glutamate receptors (mGluRs),[8] or (ii) facilitate subsequent inhibition effect through activating N-methyl-d-aspartate receptors (NMDARs).[9]

This intriguing regulatory mechanism in biological neural systems has inspired the use of neuromorphic devices to mimic the metaplasticity function across a broad range of research fields.[10,11] Many devices that mimic this intriguing synaptic metaplasticity have recently been successfully implemented in two-terminal memristors.[10−17] Some groups reported the effect of metaplasticity on the spike-timing-dependent plasticity (STDP) performance of an artificial synapse, and successfully mimicked the intriguing metaplasticity with a memristor by controlling the internal filament geometry configuration. Although these devices are very impressive, the development of metaplasticities based on novel device materials and architectures are still needed.

As a promising candidate, field-effect transistors (FETs), having an extra gate terminal, can utilize hysteresis relaxation to achieve linear and dynamic plasticity,[18−21] possibly resulting in a higher-level metaplasticity in neuromorphic devices.[22] In this work, biological bipolar metaplasticities (BBMs) were successfully mimicked in 2D MoS_2 transistors for the first time using two different MoS_2 surface decorations, poly (vinyl alcohol) (PVA) and chitosan biopolymers. Interestingly, the depressing metaplasticity was successfully mimicked when the PVA bio-polymer was used as the surface decoration layer, whereas the metaplasticity of LTP was realized when the chitosan bio-polymer was employed as the surface decoration layer. These BBMs represent a dynamic response coupled to prior activity that has the poten-

Supported by the Central South University Research Fund for Innovation-Driven Program (Grant No. 2019CX024), the Natural Science Foundation of Hunan Province (Grant No. 2018JJ3652), the China Postdoctoral Science Foundation (Grant Nos. 2018M632985 and 2018T110839), and the Fundamental Research Funds for the Central Universities of Central South University (Grant No. 2018zzts333).

*Corresponding author. Email: jiangjie@csu.edu.cn; junhe@csu.edu.cn

© 2020 Chinese Physical Society and IOP Publishing Ltd

tial via synergistic reaction to provide sophisticated regulation of plasticity across space and time and promote homeostasis.[23] More importantly, these intriguing results can be theoretically explained via the first-principle calculation owing to ion adsorption effects on the MoS_2 interface. These findings are of great importance in driving more advanced neuromorphic computations in the future.

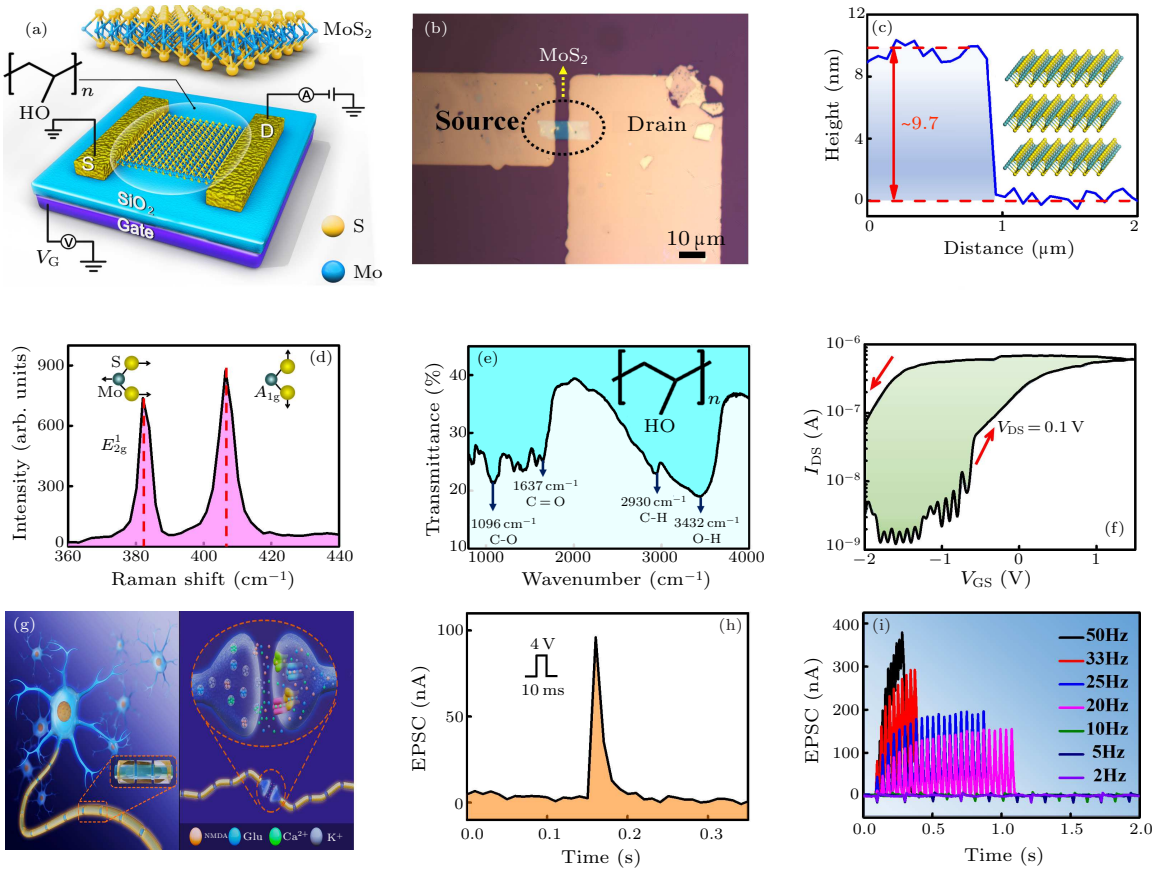

Fig. 1. (a) A schematic picture of the PVA-decorated 2D MoS_2 synaptic transistor. (b) A top-view optical image of the device. (c) AFM measurement at the edge of MoS_2 flake. Inset: the schematic diagram of the layered atomic structure of multilayer MoS_2. (d) Raman spectroscopy of the exfoliated MoS_2 flake. (e) FTIR of the PVA film. Inset: the intrinsic molecular structure of the PVA. (f) The transfer characteristic curve of the MoS_2 transistor with a fixed bias of $V_{DS} = 0.1$ V. (g) Magnified schematic diagrams of neurons (left panel) and two adjacent neurons connected by a synapse. (h) A typical EPSC response of the MoS_2 synaptic transistor triggered by a presynaptic spike (4 V, 10 ms). (i) EPSCs recorded in response to the stimulus train with different frequencies.

Figure 1(a) schematically shows the bottom-gate PVA-decorated 2D MoS_2 transistor (specific fabrication processes are provided in the following). The PVA powder is purchased from Sigma-Aldrich, and the corresponding molecular weight is about 85000–124000. In this work, to mimic an artificial synapse, PVA is chosen as the top surface decoration layer rather than a top dielectric layer. Actually, there are other amorphous polymers such as poly-α-methylstyrene, poly-methyl methacrylate, and polystyrene that can be excellent candidates of gate dielectric materials according to the literature.[24–27] Two-dimensional MoS_2-based devices have high application prospects in many of the most advanced electronic applications due to the fact that the MoS_2 material has interesting electron properties, as well as special atomically scalable structure advantages.[28,29] Figure 1(b) shows the optical top-view micrograph of the MoS_2 FET where the two nickel electrodes are connected by an MoS_2 flake. By using atomic force microscopy (AFM), the thickness of as-fabricated MoS_2 flakes is estimated to be ∼9.7 nm, as shown in Fig. 1(c). The number of MoS_2 layers in our device should be ∼15 layers, since the thickness of monolayer MoS_2 is about 0.65 nm.[30] The inset of Fig. 1(c) shows the van der Waals layered atomic structure of MoS_2. The properties of the exfoliated MoS_2 are determined from their Raman spectra, as shown in Fig. 1(d). Both in-plane mode (∼382 cm^{-1}) and out-of-plane A_{1g} mode (∼406 cm^{-1}) can be observed.[31] Compared with MoS_2 single crystal raw materials, good crystal properties are obtained in our exfoliated MoS_2 flakes.[31,32] Figure 1(e) displays the molecular structure (in the illustration) and Fourier transform infrared spectroscopy (FTIR) of the PVA membrane. Two major peaks, linked to C–H stretching at 2930 cm^{-1} and O–H stretching at 3432 cm^{-1}, are clearly observed.[32] Moreover, other two peaks

(1096 cm^{-1} and 1637 cm^{-1}) are originated by C–O and C=O stretching, respectively.[33] Figure S1(a) in the supplementary material displays the output curve (I_{DS} vs V_{DS}) of our neuromorphic device with the V_{GS} from −2 V to 2 V in steps of 1 V. The contact resistance is roughly estimated to be about $5 \times 10^4\,\Omega$ according to the output curves. At present, for the non-saturation behavior of output curves, we tend to believe that it is possibly due to the short-channel effect.[34] More specifically, for a low gate bias in the output curve, this phenomenon is possibly caused by the barrier breakdown in the source/channel interface due to the strong V_{DS} electric field in a short channel. If a large gate bias is applied, the source/channel barrier would be lower due to the increase of electron concentrations in the channel, and the output curve exhibits more like a linear-resistor characteristic in such a case. Figure 1(f) shows the transfer curve (I_{DS}–V_{GS}), with a fixed V_{DS} of 0.1 V. A clear anticlockwise hysteresis is obtained when V_{GS} steps from −2.0 to 1.5 V and then back, which is potentially due to the presence of mobile protons in the PVA bio-polymer.[35] A key characteristic of our neuromorphic device is the ability to realize a higher-order form of synaptic plasticity (metaplasticity). A magnified schematic diagram of the neurons and synapses is shown in Fig. 1(g). When the inhibitory and excitatory signals arrive, the neurotransmitters from the presynaptic neuron are released into the synaptic cleft and then arrive at the postsynaptic membrane via diffusion, resulting in an action potential in the postsynaptic neuron.[1–3] Some special neurotransmitters (glutamate and NMDA) play important roles in various complex learning, emotional, and psychological functions during this process via weight changes in the postsynaptic currents.[1,2,36] Such a biological synapse can be mimicked in our 2D neuromorphic MoS_2 transistor, where the bottom gate serves as the presynaptic input terminal and the source/drain electrodes act as postsynaptic output terminals. Figure 1(h) shows the excitatory postsynaptic current (EPSC) of the bottom-gate MoS_2 transistor triggered by a presynaptic spike (4 V, 10 ms). The triggered EPSC attained its maximum value (96.1 nA) at the end of the input spike and then gradually returned to the resting current (3.9 nA), resembling a biological excitatory synapse.[2,3] The time constant could be well fitted through an exponential equation as follows:

$$I = I_0 + I_1 \exp(-t/\tau), \tag{1}$$

where τ is the retention time constant, I_1 is the EPSC amplitude, and I_0 is the ultimate amplitude of decay current. Figure S1(b) shows a good fitting for the decay characteristic. It was obtained that τ is about ∼9 ms, which means that the characteristic time of ion migration under excitatory signals is found to be ∼9 ms. At the same time, the paired-pulse facilitation (PPF), in biological systems, is a form of short-term synaptic plasticity, and is necessary for decoding temporal information in visual or auditory signals.[37] It is a phenomenon whereby the EPSC evoked by an impulse increases when the impulse closely follows a prior impulse.[2,3,37] This typical neuron behavior reappears in our neuromorphic device, as shown in Fig. S1(c), with the PPF behavior observed when two successive spikes (4 V, 10 ms) are applied to the bottom gate (presynaptic input). It is clear that the amplitude triggered by the second presynaptic spike (337.4 nA) is obviously larger than that triggered by the first one (220.3 nA), which is possibly due to the inability of the protons to migrate back to their original state when the interval is smaller than the ionic relaxation time.[22] In biological signal processing, dynamic rate/frequency-dependent filters may further extend above the PPF behavior.[38] An observable change in the synaptic efficacy may be present after particular temporal patterns in a neural system activity occur.[2,39] Interestingly, short-term synaptic facilitation may lead to high-pass temporal filtering, which can be mimicked in our device. Figure 1(i) illustrates the EPSC responses of the bottom-gate MoS_2 transistor to pulse stimuli with different frequencies that span 2–50 Hz. The pulse stimuli at each frequency consist of a series spike train (4 V, 10 ms). It is clear that the peak value increases significantly for the high-frequency stimuli, which illustrates that a high-pass frequency filter is realized in our MoS_2 neuromorphic device. Here, the frequency-dependent gain can be defined as the ratio between the tenth EPSC (A_{10}) and the first EPSC (A_1), as shown in Fig. S1(d). Interestingly, the gain increases linearly from ≈1.05 to ≈12.77 when the stimulus frequency changes from 10 to 50 Hz. Therefore, the results presented here indicate that the 2D MoS_2 synaptic transistor can act as a good dynamic high-pass filter for information transmission. Extracting information concerning fast changes in signal amplitude and rejecting that from slow fluctuations, that is, high-pass temporal filtering, are central to the utility of the jamming avoidance response. Such a high-pass filter function mimicked here is very interesting for computing the direction of motion of an electric image and therefore directional selectivity in artificial nervous systems.[2]

In addition to the above-mentioned basic synaptic plasticity functions, the higher-order form of synaptic plasticity (metaplasticity) in biological systems is an important component of the brain learning mechanism.[5,9] This metaplasticity may increase the efficacy of both the memory and processing capacity of neurotransmitters, resulting in a great robustness and competitive characteristic of neuron weights.[4,40] The competitive winner-takes-all and Hebbian learning rules can be promoted via metaplasticity for neuromorphic computing applications (e.g., sound localization and pattern recognition).[39] Interestingly, bipolar metaplasticities, which are inspired by the existence of metaplasticity in biological systems, are successfully

mimicked in our MoS_2 transistors. We use the SiO_2 as the bottom gate, so that the MoS_2 channel can be exposed to the outside and well decorated, which is beneficial to the emulation of our biological functions. Actually, the top-contact structure is facile for the fabrication process and that is also our next research direction.

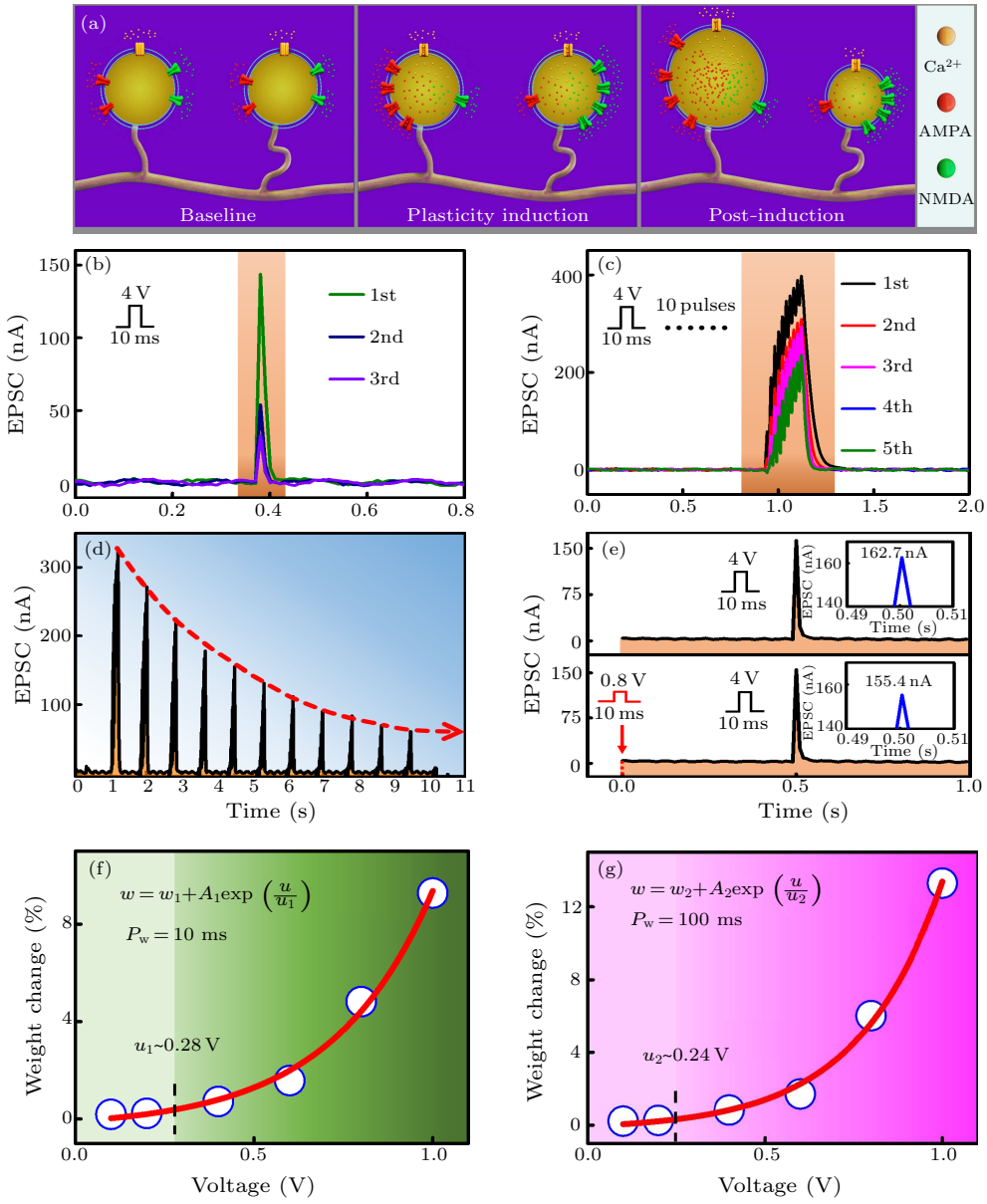

Fig. 2. (a) The schematic diagram for two different forms of metaplasticity. (b) Three continuous transient EPSC responses measured with the same spiking stimulus (4 V, 10 ms). (c) The EPSC triggered by the successive gate electric spikes with the same amplitudes (4 V, 10 ms) five times. (d) The EPSC triggered by applying sequential 11 spiking stimuli with an amplitude of 4 V, a width of 10 ms, and an interval of 0.6 s. (e) Typical depressing metaplasticity phenomenon. (f) Apply the priming spikes with different amplitude for examining its influence on the subsequent depressing metaplasticity. (g) Apply priming spikes with different widths for examining its influence on the subsequent depressing metaplasticity.

Figure 2(a) shows the schematic diagram for two different forms of metaplasticity whereby the special neurotransmitters (Ca^{2+}, glutamate, and NMDA) play a critical role.[41] The primary state of the synapses is displayed in the left panel, where Ca^{2+}, α-amino-3-hydroxy-5-methyl-4-isoxazole propionic acid (AMPA), NMDA, and other neurotransmitters are all outside of the synaptic membrane. A typical metaplasticity of LTP occurs when the increase in AMPA receptors leads to modulation of the neurotransmitter (AMPA > NMDA) and more Ca^{2+} influxes into the synaptic membranes.[7,42] However, increasing the NMDARs yields a varied neurotransmitter (NMDA > AMPA) and less Ca^{2+} influxes into the synaptic membranes would result in a depressing metaplasticity,[8] as shown in the right panel of Fig. 2(a). Interestingly, our 2D MoS_2 transistor with a PVA bio-polymer can successfully realize the depres-

sion metaplasticity. Figure 2(b) illustrates three transient EPSC responses that were measured repeatedly under the same amplitudes of the gate electric spikes (4 V, 10 ms). An interesting result can be observed from this figure: the EPSC responses decreased from 143.7 to 32.7 nA with the repeated stimuli, which indicates that our device has the typical characteristic of inhibition.[42] This phenomenon is further confirmed in Fig. 2(c), EPSC of MoS_2 neuromorphic transistor was reduced from 398.1 to 235.5 nA triggered by stimulus train with 10 pulses (4 V, 10 ms) (continuously repeated the measurements with five times). The EPSC response was then triggered using eleven sequential stimulus spikes (spike amplitude: 4 V, spike width: 10 ms, spike interval: 0.6 s), as shown in Fig. 2(d), to further study these inhibition effects. An interesting result can be observed from this figure, with continuous spiking stimuli, it is clear that the resulted EPSC gradually decrease from 326.1 to 60.6 nA and get saturated, as shown by the red dashed line in Fig. 2(d). This phenomenon indicates that the transient dynamic of our device exhibits an obvious inhibition memory. In biological systems, such a phenomenon is thought to play an important role in subsequent memory formation and learning, reflecting the possible changes in the central nervous system related to lasting memory.[43,44] Based on the unique property of our device, a depressing metaplasticity is shown in Fig. 2(e). The control experiment, where a single-voltage pulse is applied (upper panel), shows the difference between metaplasticity and conventional synaptic plasticity. The EPSC immediately attains its maximum value (162.7 nA) via a presynaptic spike stimulus (4 V, 10 ms). The probes that are connected to the electrodes are then suspended (∼3 min) to enable the device to return to its original equilibrium state. Conversely, a priming weak spike (0.8 V, 10 ms) triggers a 155.4 nA EPSC from the succedent main voltage pulse (4 V, 10 ms). The lower EPSC peak (155.4 versus 162.7 nA) is observed in our device, which indicates that the priming stimulus successfully regulated the synaptic plasticity. Furthermore, the synaptic weights of metaplasticity can be evaluated by the change of EPSC as follows:

$$w = (E_1 - E_0)/E_0, \tag{2}$$

where w is the synaptic weight, and E_0 and E_1 are the relative EPSC values before and after the weak priming spike are applied, respectively. A weak priming stimulus can also generate an EPSC by itself in our devices, which is analogous to biological systems. It is generally difficult to distinguish between metaplasticity and conventional plasticity since the priming stimulus can sometimes change the ability to produce plasticity.[4,23] A study of the nervous system has reported that inhibition effect can be obtained when postsynaptic depolarization exceeds a critical value,[45] with the NMDAR playing an important role in inducing subsequent inhibition. The threshold of the plasticity relies to the cell's previous history of stimulus, according to Bienenstock, Cooper, and Munro (BCM) theory.[40] In other words, when the priming spike triggers postsynaptic depolarization, the subsequent inhibition will be induced. At the same time, the NMDA receptor activation lowers the threshold for inhibition.[9,44–46] Therefore, we applied priming spikes with different amplitudes to investigate their influence on subsequent inhibition effect, as shown by the empty circular symbols in Fig. 2(f). These results illustrate that the amplitude of the priming spike can effectively modulate the subsequent metaplasticity. A synaptic weight change of up to 9.3% is obtained when the priming spiking amplitude increases to 1 V. These experimental results also fit the following equation:

$$|w| = w_1 + A_1 \exp\left(\frac{u}{u_1}\right), \tag{3}$$

where w_1 and A_1 are different weight constants, and u_1 is the characteristic voltage constant related to the subsequent metaplasticity. Here we obtain a best-fit solution for $u_1 \approx 0.28$ V, which indicates that the significant metaplasticity phenomenon can be observed when the priming spike is larger than u_1. Therefore, we define a threshold stimulus amplitude of $V_{T1} \approx 0.28$ V to distinguish between the generations of typical metaplasticity and conventional plasticity. A larger pulse width of 100 ms is applied to the priming stimulus to further investigate the threshold characteristic of metaplasticity. Figure 2(g) shows the experimental data (empty circular symbols) and fitted results (solid line), with a good fit obtained when the synaptic weight change is

$$|w| = w_2 + A_2 \exp\left(\frac{u}{u_2}\right), \tag{4}$$

where w_2 and A_2 are different weight constants, and u_2 is a characteristic voltage constant (best fit when $u_2 \approx 0.24$ V), indicating that the metaplasticity threshold of $V_{T2} \approx 0.24$ V is smaller than V_{T1} (0.28 V). This phenomenon reveals that the subsequent metaplasticity threshold decreases with the increasing priming spike width. Therefore, the metaplasticity threshold can be adjusted by changing the width of the priming stimulus, yielding the results that are very similar to the metaplasticity behavior in the biological nervous system. It has been reported that the psychological tactile spatial sensitivity of professional pianists is very different from that of nonmusicians,[47] with long-term piano practice leading to a lower spatial discrimination threshold, which indicates a form of metaplasticity in professional pianists. This type of metaplasticity suggests somatosensory information processing that is beyond training-specific constraints, i.e., reduced spatial discrimination threshold through sustained training.[23,47]

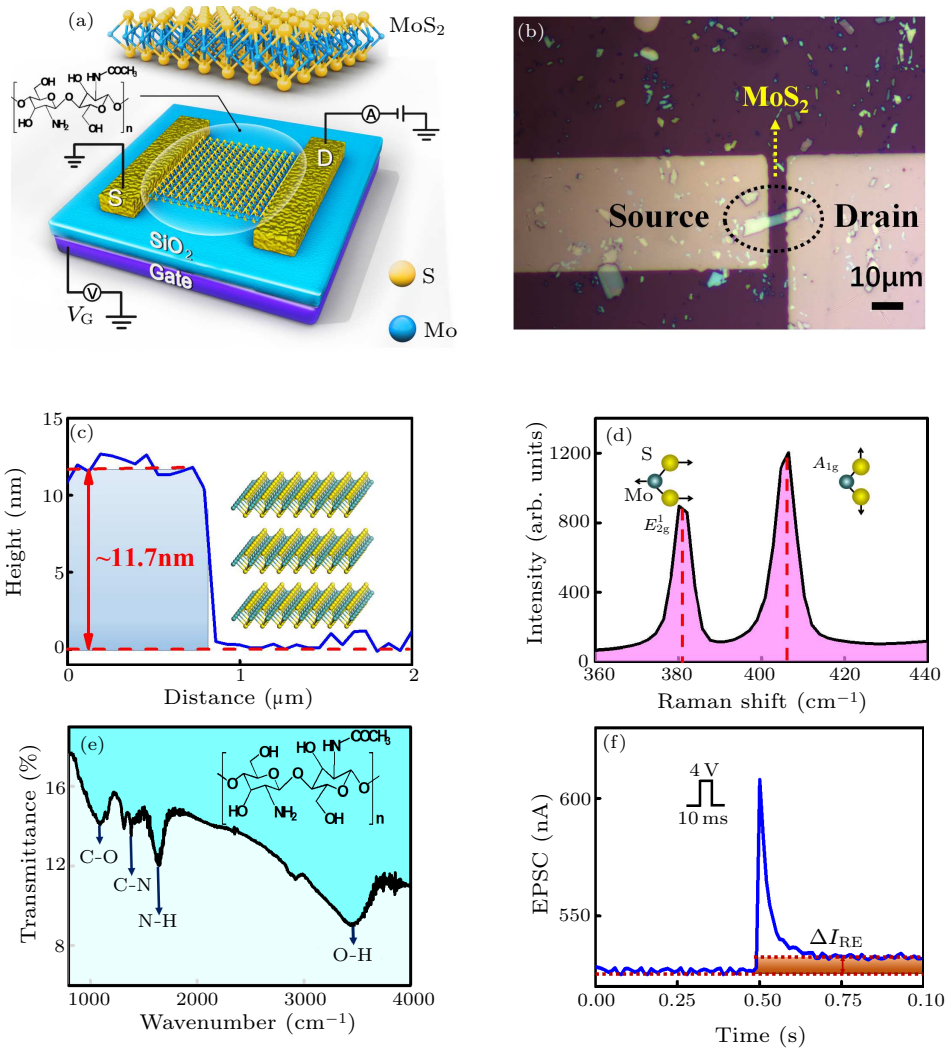

Fig. 3. (a) A schematic picture of the chitosan-decorated 2D MoS_2 synaptic transistor. (b) A top-view optical image of the device. (c) AFM measurement at the edge of MoS_2 flake. Inset: schematic diagram of layered atomic structure of multilayer MoS_2. (d) Raman spectroscopy of the exfoliated MoS_2 flake. (e) FTIR of chitosan film. Inset: the intrinsic molecular structure of the chitosan. (f) EPSC triggered by a presynaptic pulse (4 V, 10 ms).

In biological systems, in addition to the inhibition effect, the LTP is also another important mechanism closely related to basic memory and learning occurring in the central nervous system.[3] Our neuromorphic device, which is based on a 2D MoS_2 transistor with a chitosan bio-polymer, can successfully realize this important metaplasticity of LTP. The schematic diagram of the device structure is shown in Fig. 3(a), with an optical top-view micrograph of the MoS_2 device shown in Fig. 3(b), where two nickel electrodes (source and drain) are connected by a MoS_2 flake. The thickness of the MoS_2 flake is ∼11.7 nm via AFM, as shown in Fig. 3(c). Therefore, there should be ∼18 layers based on a 0.65 nm thickness per layer value.[23] The inset of Fig. 3(c) displays a schematic diagram of the van der Waals layered atomic structure of the MoS_2 flake. The properties of the exfoliated MoS_2 were determined from the Raman spectra, as shown in Fig. 3(d). Both the in-plane (380 cm^{-1}) and out-of-plane A_{1g} (∼404 cm^{-1}) modes can be observed in the MoS_2 flake, indicating that our exfoliated MoS_2 flake has good crystal properties compared to a single MoS_2 crystal.[31,32] The FTIR spectra of the chitosan membrane reveal its major chemical bonds and molecular structure, as shown in Fig. 3(e). The peak at ∼3440 cm^{-1} is attributed to the O–H group,[48] and the characteristic absorption band at 1660 cm^{-1} is due to N–H bending vibrations. Two peaks are also visible at 1380 and 1080 cm^{-1}, which are due to the C–N and C–O groups, respectively.[48,49] The corresponding transfer curve (I_{DS}–V_{GS}) and output curve (I_{DS}–V_{DS}) are provided in Figs. S2(a) and S2(b), respectively. The field-effect mobility μ can be extracted from the equation

$$\mu = \frac{L}{C_i \times W \times V_{DS}} \times \frac{dI_{DS}}{dV_{GS}}, \tag{5}$$

where $L = 6\,\mu m$ is the channel length, $W = 9\,\mu m$ is the channel width, the SiO_2 dielectric capacitance is 1.2×10^{-8} F/cm^2 (ε_0 is the dielectric constant of vacuum, ε_r is the relative dielectric constant of SiO_2 ($\varepsilon_r = 3.9$), and d is the thickness of the gate insu-

lator (300 nm)). Therefore, the μ is calculated to be 5.83 cm^2/Vs for the pristine state, 69.3 cm^2/Vs for the –OH adsorption state (PVA-decorating device), and 55.1 cm^2/Vs for the H^+ adsorption state (chitosan-decorating device), respectively. The EPSC is triggered by applying a presynaptic spike (4 V, 10 ms) on the bottom gate of the MoS_2 transistor, with a reading voltage of $V_{DS} = 0.1$ V applied between the drain and source electrodes during the test.

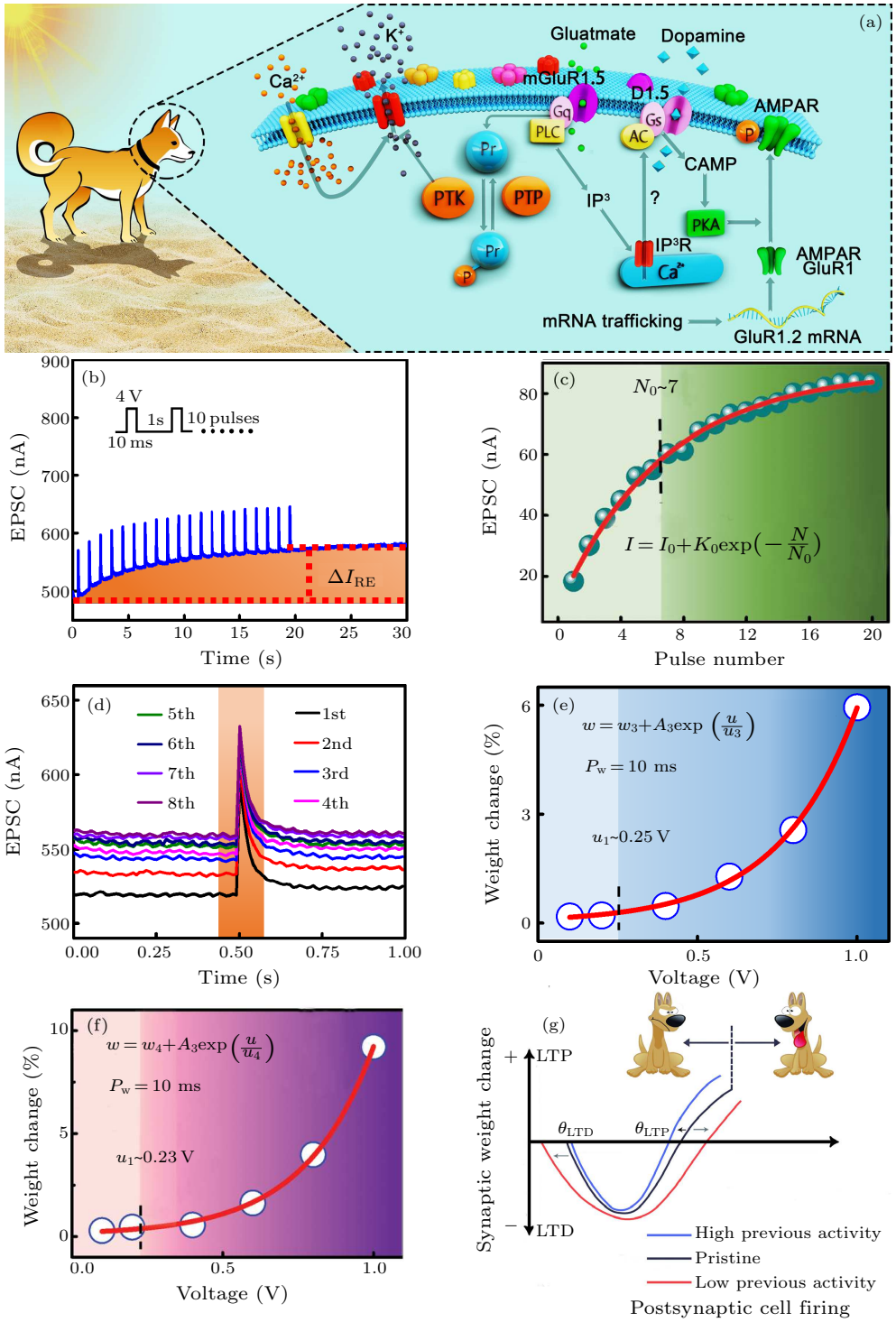

Fig. 4. (a) The schematic diagram of metaplasticity of LTP. (b) A series of 20 single pluses are applied with an amplitude of 4 V, a width of 10 ms, and an interval of 1 s to trigger EPSC responses. (c) EPSCs changed with the increase of pulse number. (d) Eight transient EPSC responses measured repeatedly under the same amplitudes of electric spikes (4 V, 10 ms) for the gate terminal. (e) Apply the priming spike with different amplitude for examining its influence on the subsequent metaplasticity of LTP. (f) Apply the priming spike with different widths for examining its influence on the subsequent metaplasticity of LTP. (g) A schematic diagram revealing the relationship between the plasticity, metaplasticity of LTD, and metaplasticity of LTP.

Interestingly, the triggered EPSC at the end of the input spike attained a maximum value of 607.9 nA, but the resting EPSC did not return to its initial current state (528.3 nA) during the test, as shown in Fig. 3(f). From this figure, the resting EPSC difference before and after spike stimulus ($\Delta I_{\rm RE}$) is found to be 5.2 nA, indicating that the long-term memory (LTM) is successfully implemented by our neuromorphic bottom-gate MoS_2 device. LTM is the most important form of plasticity among the many synaptic properties of mammalian brains.[50] The electrical response of the neurons can be enhanced via continuous modification of the synaptic weight, resulting in biological LTM behavior. Our result provides clear evidence of LTM in our neuromorphic MoS_2 device. A similar LTM effect is also observed in the PPF measurements, as shown in Fig. S3(a). Here the EPSCs are triggered by applying a pair of presynaptic spikes (spike amplitude 4 V, spike width 10 ms, spike interval 10 ms), whereas the resting EPSC does not return to its initial current state, and a larger $\Delta I_{\rm RE}$ is observed (10.4 nA), which further confirms that our neuromorphic MoS_2 device can successfully mimic this intriguing LTM behavior.

Compared with the potentiation effects of NMDARs priming on inhibition in area CA1, the induction of subsequent LTP is activated by group-1 mGluRs,[7] as shown in Fig. 4(a). The mGluR activation inhibits the Ca^{2+}-activated K^+ channel, which mediates the slow afterhyperpolarization current.[51] The phosphorylation state of an unknown regulatory protein (phosphoprotein, Pr) can regulate this process,[52] with the stimulation of phospholipase C and intracellular release of Ca^{2+} activating protein kinase A and adenylyl cyclase, respectively, to induce subsequent LTP.[53] Most importantly, the trafficking of AMPARs to the extrasynaptic membrane can enhance induction of metaplasticity of LTP.[54] This process also depends on the enhancement of AMPAR-subunit mRNA trafficking to the synaptic sites. Here we successfully mimicked this higher-order form of synaptic plasticity (metaplastic facilitation of LTP) in the bottom-gate MoS_2 transistor using chitosan biopolymer as the surface decoration layer. The neuromorphic device is triggered by a 20-spike stimulus train (spike amplitude 4 V, spike width 10 ms, spike interval 1 s), as shown in Fig. 4(b), with a gradual increase in EPSC that eventually becomes saturated after the successive stimuli. The resting current does not return to its initial state (∼486.3 nA) when the spike is interrupted, but rather continues to maintain a high ESPC of 572.8 nA ($\Delta I_{\rm RE} \approx 86.5$ nA). Here the EPSC dependence with the pulse number can be summarized with the Fig. 4(c). A significant synaptic weight potentiation is observed with each stimulus that gradually becomes saturated after applying the 20-spike stimulus train, indicating that the chitosan-decorated MoS_2 device successfully mimics a strong LTP phenomenon. A good fit (solid line) to the experimental data (solid circular symbols) is obtained by

$$I = I_0 + K_0 \exp\Big(-\frac{N}{N_0}\Big), \tag{6}$$

where I is the EPSC increment, I_0 and K_0 are the different weight constants, and N_0 is the characteristic pulse number constant. The best-fit solution is obtained for $N_0 \sim 7$, which indicates that the LTP phenomenon approaches saturation when $N_0 > 7$. I will reach its saturated state I_0 (∼87.7 nA) as $N \to \infty$, which is the maximum LTP value that the device can attain. In mammalian brains, long-term potentiation reflecting the possible synaptic weight changes in the central nervous system is the most important form of plasticity among many synaptic properties. It plays important roles in various complex learning, emotional and psychological functions.[55] Such biological behavior can be further demonstrated via the successful application of an eight-spike stimulus train (4 V, 10 ms) to the bottom-gate terminal in Fig. 4(d). Interestingly, the resultant EPSC peaks increase from 594.8 to 632.2 nA, and the corresponding resting current also increases from 519.2 to 559.1 nA after these eight successive stimuli. Figure S3(b) further exhibits the EPSC response triggered by seven successive measurements of a ten-spike stimulus train, with a significant synaptic weight potentiation clearly observed during each spike-train measurement and the resultant EPSC peaks increasing from 675.3 to 696.4 nA. Furthermore, the resting EPSCs before and after the seven ten-spike stimulus trains also increase from 509.2 to 538.1 nA. These results strongly indicate that our MoS_2 neuromorphic transistor exhibits a clear LTP phenomenon. LTP in the human brain reflects the possible synaptic weight changes in the central nervous system, which are related to LTM.[56] The activation of mGluRs is therefore of great importance for mediating LTP-enhanced synaptic responses during this process.[7,56] Based on the unique property of our device, the metaplasticity of LTP is shown in Fig. S3(c). The upper panel illustrates that the EPSC attains its maximum value (570.7 nA) when triggered by a presynaptic spike (4 V, 10 ms). The probes connected to the electrodes are then suspended (∼3 min) to ensure that the device will restore to its original equilibrium state. The lower panel illustrates that a weak priming spike (0.8 V, 10 ms) causes a 573.6 nA EPSC to be triggered by the succedent main voltage pulse (4 V, 10 ms). Our device attains a higher EPSC (573.6 versus 570.7 nA) compared to the synaptic plasticity in the upper panel. Here we employ a priming spike with different amplitudes (0.1–1 V) before the main spike stimulus (4 V, 10 ms) to determine this metaplasticity of LTP, as shown in Fig. 4(e). A good fit (solid line) to these experimental results (empty circular symbols) is obtained when the synaptic weight change is

$$w = w_3 + A_3 \exp\Big(\frac{u}{u_3}\Big), \tag{7}$$

where w_3 and A_3 are different weight constants, and u_3 is the characteristic voltage constant related to the subsequent metaplasticity. We obtain a best-fit solution for $u_3 \approx 0.25\,\mathrm{V}$, which indicates that the significant metaplasticity phenomenon can be observed when the priming spike is larger than u_3. This result also indicates that a threshold stimulus amplitude of $V_{\mathrm{T3}} \approx 0.25\,\mathrm{V}$ exists in the generation of metaplasticity, such that the subsequent metaplasticity can be clearly observed once the amplitude of the previous weak spike exceeds this threshold. Previous studies have employed BCM theory to illustrate the activity-dependent regulation of the LTP threshold.[57] Pharmacological disinhibition or intracellular current injection stimuli in the biological nervous system can modify the depolarizing level and then induce LTP production,[23] while mGluR activation can lower the LTP threshold.[45] A larger pulse width of 100 ms is applied to the priming spike to realize this biological behavior. Figure 4(f) shows the experimental data (empty circular symbols) and fitted results (solid line), with a good fit obtained when the synaptic weight change is

$$w = w_4 + A_4 \exp\left(\frac{u}{u_4}\right), \tag{8}$$

where w_4 and A_4 are different weight constants, and u_4 is characteristic voltage constant (best fit when $u_4 \approx 0.23\,\mathrm{V}$), indicating that the metaplasticity threshold of $V_{\mathrm{T4}} \approx 0.23\,\mathrm{V}$ is smaller than V_{T3} (0.25 V). This phenomenon reveals that the subsequent metaplasticity threshold decreases with increasing priming spike width. Therefore, the metaplasticity threshold can be adjusted by changing the width of the priming stimulus, yielding results that are very similar to the metaplasticity behavior in the biological nervous system. The subsequent metaplasticity threshold decreases with increasing priming spike width, indicating that the ability to produce metaplasticity of LTP is effectively enhanced. These results are very similar to the metaplasticity behavior in the nervous system, where the activated mGluRs can lower the LTP threshold.[45] Similar measurements are also performed to investigate the existence of this metaplasticity phenomenon using the bottom-gate MoS_2 transistor without surface polymer decoration (details are shown in Figs. S4 and S5), with neither the basic EPSC effect nor the metaplasticity phenomenon observed after five successive stimulus-train measurements. Learning in the human brain can be regulated through the change of synaptic weights, such as LTD and LTP.[58] Interestingly, both LTD and LTP can be dynamically modulated by the prior activity in the biological system (metaplasticity). Figure 4(g) shows the relationship between plasticity and metaplasticity. The black (control) curve shows the postsynaptic cellular response at different levels to the excitatory synapses in hippocampal CA1 pyramidal cells,[44] where θ_{LTP} and θ_{LTD} represent the postsynaptic firing thresholds required by afferent stimulation to produce LTP or LTD, respectively. The red and blue lines represent the effects of the priming stimuli on the subsequent LTD and LTP, respectively. Specifically, mGluR activation (blue curve) raises the LTD threshold and lowers the LTP threshold, whereas the NMDAR activation (red curve) lowers the LTD threshold.[45,46] Therefore, the ability of synaptic plasticity to undergo persistent potentiation or depression can be profoundly altered by previous neuronal activities, i.e., metaplasticity of LTP or depressing.[59] Compared to the unipolar metaplasticities, the main advantages of bipolar metaplasticities may include, but are not restricted to, synchronization control of neural network excitability, such that synaptic efficacy is maintained within the range of operation[23] Some diseases, such as depression, attention deficit hyperactivity disorder, post-traumatic stress disorder, and schizophrenia, can even be controlled due to the interesting regulatory mechanism.[60] Therefore, it is promising that the use of neuromorphic devices to mimic these fascinating biological behaviors could greatly expand artificial neural network applications and provide new bio-realistic neuromorphic computing approaches.

In order to further investigate the underlying mechanism of BBMs in our neuromorphic devices, the electronic band structure of 2D MoS_2 with different surface polymer decorations (PVA or chitosan) can be investigated using the first principle calculations.[61] The current method is realized by the Vienna ab initio simulation package (VASP) code, depending on density functional theory (DFT).[62] In the calculation, a plane-wave cut-off of 450 eV is used. The Brillouin zone was sampled by a Monkhorst–Pack $6 \times 6 \times 1$ k-point grid. All of the atoms are allowed to relax until the Hellmann–Feynman force was below 0.01 eV/Å. In the self-consistent process, the energy convergence criterion is approximately 1×10^{-4} eV.[62,63] Figure 5(a) shows the charge density difference, the yellow and red represent electron depletion and accumulation. It is clearly observed that the surface charge distribution of MoS_2 is strongly affected by the surface functional groups (PVA or chitosan bio-polymer). More specifically, in the left panel of Fig. 5(a), many charged holes are trapped on the surface of layered MoS_2 crystal due to the adsorption of –OH in PVA bio-polymer. However, MoS_2 is a well-known n-type semiconductor and its electrons are majority carriers.[64] Therefore, the adsorbed holes indicate electron depletion on the MoS_2 surface, resulting in a continuous decrease in the channel current. Conversely, the H^+ in chitosan bio-polymer would induce many electrons in the surface of MoS_2, indicating that larger channel currents can be obtained as shown in the right panel of Fig. 5(a). Furthermore, the electronic band structures of the pristine state on the MoS_2 surface, the –OH, and H^+ adsorption states, can be systematically compared, as shown in Fig. 5(b). The typical semiconductor property of pristine MoS_2, with a

bandgap of ∼1.68 eV, can be found in the left panel, which is in good agreement with a previous study.[65] It should be noted that, in the middle panel, the Fermi level in the band structure would shift toward the valence band when the MoS_2 surface is decorated with a PVA bio-polymer. Therefore, the low conductance state can be obtained in our neuromorphic device, which is in good agreement with the depressing metaplasticity. Interestingly, the Fermi level in the band structure will shift toward the conduction band when the MoS_2 surface is decorated with the chitosan bio-polymer, resulting in a high conductance state, as shown in the right panel of Fig. 5(b). This phenomenon is highly consistent with the metaplasticity of LTP which exhibits continuous enhancement after successive stimuli. A cross-sectional schematic diagram is proposed to explain such depression and potentiation effects via surface polymer decoration to intuitively understand the above-mentioned BBMs in an MoS_2 synaptic transistor, as shown in Fig. 5(c). Compared with the pristine state, the –OH group in the PVA bio-polymer can be regarded as a negatively charged group, which would induce electron reduction on the MoS_2 surface. However, the H^+ in the chitosan bio-polymer would result in electron accumulation on the MoS_2 surface, such that a higher conductance state is observed. The bottom-gate MoS_2 device without any surface polymer decoration is also fabricated to further confirm the rationality of our conjecture, with no clear metaplasticity observed (Fig. S5). Such functional-group induction effects from the opinion of first-principles calculations can be well utilized to understand the variation of channel conductance, i.e., the implementation of surface polymer decoration in the above-mentioned BBMs. Some special neurotransmitters (glutamate, and NMDA) play important roles in the generation of bipolar metaplasticities in biological nervous systems.[41] This intriguing phenomenon can allow the modified synaptic network to remain in a useful dynamic range and promote homeostasis.[23,66] Therefore, the demonstration of BBMs in our device is a key step in the development of next-generation neuromorphic electronics.

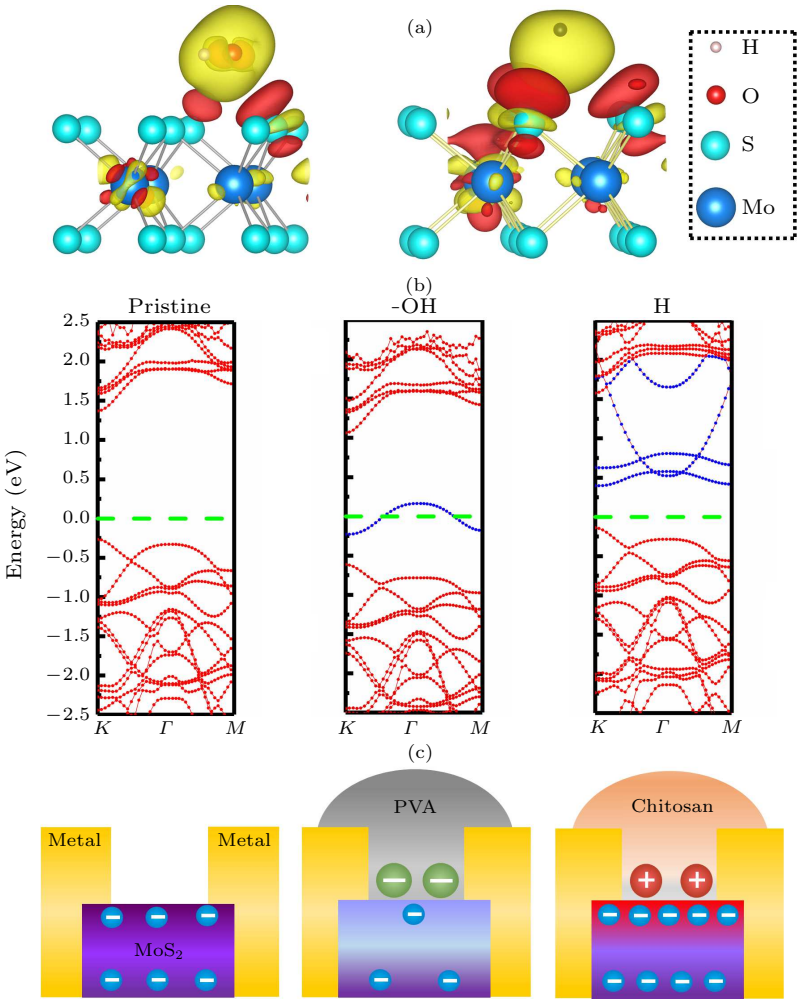

Fig. 5. (a) The charge density difference of MoS_2 adsorbed OH ion and H ion. Left panel: MoS_2 surface functionalized by –OH group from PVA bio-polymer. Right panel: MoS_2 surface functionalized by H^+ from chitosan bio-polymer. (b) The electronic band structures of MoS_2 surface under the pristine state, –OH adsorption state, and H^+ adsorption state, respectively. (c) Cross-sectional schematic diagram of charge distribution of the MoS_2 transistor under the pristine state, –OH adsorption state, and H^+ adsorption state, respectively.

In summary, we have experimentally demonstrated the BBMs of 2D bottom-gate MoS_2 neuromorphic transistors using different surface decorations, PVA and chitosan bio-polymers. It is found that the amplitude and width of the priming spikes can significantly affect the EPSC response, thereby regulating the generation of metaplasticity in the MoS_2 neuromorphic transistors. Such features are very similar to those in biological nervous systems, where the degree and polarity of synaptic metaplasticity can be effectively modulated. Furthermore, to better understand the underlying physics of BBMs in our neuromorphic devices, the electronic band structure of 2D MoS_2 with different surface polymer decorations have been systematically investigated by the first-principle calculation. The realization of bionic metaplasticity may alleviate many network hierarchy problems associated with statistical changes between the neuronal and synaptic elements. This work will not only deepen our understanding of the potential mechanisms of nanoscale ionic devices but also provide new insight into neuromorphic engineering.

Experimental Details. Multilayer MoS_2 flakes were first exfoliated from a bulk crystal using Scotch tape and then transferred onto a heavily doped silicon substrate with 300-nm-thick thermally-grown SiO_2. Ni (∼30 nm thickness) was subsequently deposited to form the drain and source electrodes via photolithography (photoresist: PR1-2000A1), thermal evaporation (vacuum pressure: 10^{-4} Pa), and lift-off process (∼30 min). PVA powder (Sigma-Aldrich) was then dissolved in pure water (10 wt%) at 70℃ to prepare the PVA solution. Finally, the PVA solution was drop-casted onto the MoS_2 channel as the surface decoration layer. The fabrication process was duplicated for the second device, with the only difference so that a chitosan solution (2 wt% in acetic acid) was drop-casted onto the 2D MoS_2 channel as the surface decoration layer. PVA and chitosan are ideal material candidate gate dielectrics due to their low cost, non-toxicity, biodegradability, and excellent film-forming properties.

FTIR of PVA and chitosan film were tested through an equipment of NICOLET 6700 FT-IR. The morphology and thickness of MoS_2 were measured by AFM equipment (Agilent 5500 SPM). The Raman spectroscopy was obtained by LABRAM ARAMIS. Using a semiconductor parameter characterization system (Keithley4200SCS), the electrical properties and biological synaptic functions of neuromorphic devices were tested at room temperature with the relative humidity of 50%. The presynaptic stimulus was applied on the bottom-gate electrode and the postsynaptic current was monitored using a small read voltage between the drain electrode and source electrode. Our biomimetic tests were all carried out after the solution was dried.

References

[1] Feng G, Jiang J, Zhao Y, Wang S, Liu B, He J and Wan Q 2020 *Adv. Mater.* **32** 1906171
[2] Jiang J, Guo J, Wan X, Yang Y, Xie H, Niu D, Yang J, He J, Gao Y and Wan Q 2017 *Small* **13** 1700933
[3] MacDonald J F, Jackson M F and Beazely M A 2007 *Biochim. Biophys. Acta - Biomembr.* **1768** 941
[4] Abraham W C and Bear M F 1996 *Trends Neurosci.* **19** 126
[5] Thompson R F 1986 *Science* **233** 941
[6] Sehgal M, Song C, Ehlers V L and Moyer J R 2013 *Neurobiol. Learn. Mem.* **105** 186
[7] Hulme S R, Jones O D, Raymond C R, Sah P and Abraham W C 2014 *Philos. Trans. R. Soc. B. Biol. Sci.* **369** 20130148
[8] Cohen A and Abraham W C 1996 *J. Neurophysiol.* **76** 953
[9] Christie B R and Abraham W C 1992 *Neuron* **9** 79
[10] Zhu X, Du C, Jeong Y and Lu W D 2017 *Nanoscale* **9** 45
[11] Lee T H, Hwang H G, Woo J U, Kim D H, Kim T W and Nahm S 2018 *ACS Appl. Mater. & Interfaces* **10** 25673
[12] Liu B, Liu Z, Chiu I S, Di M, Wu Y, Wang J C and Lai C S 2018 *ACS Appl. Mater. & Interfaces* **10** 20237
[13] Kim B Y, Hwang H G, Woo J U, Lee W H, Lee T H, Kang C Y, Nahm S 2017 *NPG Asia Mater.* **9** e381
[14] Tan Z, Yang R, Terabe K, Yin X, Zhang X and Guo X 2016 *Adv. Mater.* **28** 377
[15] Wu Q, Wang H, Luo Q, Banerjee W, Cao J, Zhang X and Liu M 2018 *Nanoscale* **10** 5875
[16] Cheng C, Li Y, Zhang T, Fang Y, Zhu J, Liu K and Huang R 2018 *J. Appl. Phys.* **124** 152103
[17] Mazur T, Zawal P and Szaciłowski K 2019 *Nanoscale* **11** 1080
[18] Jiang J, Hu W, Xie D, Yang J, He J, Gao Y and Wan Q 2019 *Nanoscale* **11** 1360
[19] Hu W, Zheng Z and Jiang J 2017 *Org. Electron.* **44** 1
[20] Hu W, Jiang J, Xie D, Wang S, Bi K, Duan H and He J 2018 *Nanoscale* **10** 14893
[21] Guo J, Jiang J, Zheng Z and Yang B 2017 *Org. Electron.* **40** 75
[22] John R A, Liu F, Chien N A, Kulkarni M R, Zhu C, Fu Q and Mathews N 2018 *Adv. Mater.* **30** 1800220
[23] Abraham W C 2008 *Nat. Rev. Neurosci.* **9** 387
[24] Asare-Yeboah K, Bi S, He Z and Li D 2016 *Org. Electron.* **32** 195
[25] He Z, Shaik S, Bi S, Chen J and Li D 2015 *Appl. Phys. Lett.* **106** 183301
[26] He Z, Chen J and Li D 2019 *Soft Matter* **15** 5790
[27] He Z, Zhang Z, Asare-Yeboah K and Bi S 2019 *J. Mater. Sci.: Mater. Electron.* **30** 14335
[28] Xu H F, Cui J, Sun W and Guo X F 2019 *Chin. Phys. B* **28** 108501
[29] Liu Y, Liu K, Chen R S, Liu Y R, En Y F and Li B 2017 *Chin. Phys. Lett.* **34** 018501
[30] Radisavljevic B, Radenovic A, Brivio J, Giacometti V and Kis A 2011 *Nat. Nanotechnol.* **6** 147
[31] Li H, Zhang Q, Yap C C R, Tay B K, Edwin T H T, Baillargeat A and Olivier D 2012 *Adv. Funct. Mater.* **22** 1385
[32] Kuzum D, Yu S and Wong H S 2013 *Nanotechnology* **24** 382001
[33] Sudhamani S R, Prasad M S and Sankar K U 2003 *Food Hydrocolloids DSC FTIR* **17** 245
[34] Sarker B K and Khondaker S I 2012 *Appl. Phys. Lett.* **100** 023301
[35] Xie D, Hu W and Jiang J 2018 *Org. Electron.* **63** 120
[36] Wang J, Chen Y, Kong L, Fu Y, Gao Y and Sun J 2018 *Appl. Phys. Lett.* **113** 151101
[37] Feng G, Zhao Y and Jiang J 2019 *Solid-State Electron.* **153** 16
[38] John R A, Ko J, Kulkarni M R, Tiwari N, Chien N A, Geok N, Leong W L and Mathews N 2017 *Small* **13** 1701193
[39] Jackman S L and Regehr W G 2017 *Neuron* **94** 447
[40] Sheridan P M, Cai F, Du C, Ma W, Zhang Z and Lu W D 2017 *Nat. Nanotechnol.* **12** 784

[41] Bienenstock E L, Cooper L N and Munro P W 1982 *J. Neurosci.* **2** 32
[42] Malenka R C and Bear M F 2004 *Neuron* **44** 5
[43] Zhao Y, Feng G and Jiang J 2020 *Solid-State Electron.* **165** 107767
[44] Dudek S M and Bear M F 1992 *Proc. Natl. Acad. Sci. USA* **89** 4363
[45] Artola A, Bröcher S and Singer W 1990 *Nature* **347** 69
[46] Hulme S R, Jones O D, Ireland D R and Abraham W C 2012 *J. Neurosci.* **32** 6785
[47] Ragert P, Schmidt A, Altenmüller E and Dinse H R 2004 *Eur. J. Neurosci.* **19** 473
[48] Zhao D L, Wang X X, Zeng X W, Xia Q S and Tang J T 2009 *J. Alloys Compd.* **477** 739
[49] Depan D, Girase B, Shah J S and Misra R D K 2011 *Acta Biomater.* **7** 3432
[50] Park Y and Lee J S 2017 *ACS Nano* **11** 8962
[51] Cohen A S, Coussens C M, Raymond C R and Abraham W C 1999 *J. Neurophysiol.* **82** 3139
[52] Ireland D R, Guevremont D, Williams J M and Abraham W C 2004 *J. Neurophysiol.* **92** 2811
[53] Ireland D R and Abraham W C 2002 *J. Neurophysiol.* **88** 107
[54] Oh M C, Derkach V A, Guire E S and Soderling T R 2006 *J. Biol. Chem.* **281** 752
[55] Crestani A P, Krueger J N and Barragan E V 2019 *Neuropsychopharmacology* **44** 408
[56] Bliss T V and Collingridge G L 1993 *Nature* **361** 31
[57] Abraham W C and Tate W P 1997 *Prog. Neurobiol.* **52** 303
[58] Abbott L F and Nelson S B 2000 *Nat. Neurosci.* **3** 1178
[59] Xu Z, Chen R Q, Gu Q H, Yan J Z, Wang S H, Liu S Y and Lu W 2009 *J. Neurosci.* **29** 8764
[60] Gamo N J and Arnsten A F 2011 *Behav. Neurosci.* **125** 282
[61] Van de Walle C G and Neugebauer J 2004 *J. Appl. Phys.* **95** 3851
[62] Liu B, Long M, Yang J and Cai M Q 2018 *Appl. Phys. Lett.* **112** 043901
[63] Liu B, Long M, Cai M Q and Yang J 2018 *J. Phys. D* **51** 105101
[64] Novoselov K S, Jiang D, Schedin F, Booth T J, Khotkevich V V, Morozov S V and Geim A K 2005 *Proc. Natl. Acad. Sci. USA* **102** 10451
[65] Yin Z, Li H, Li H, Jiang L, Shi Y, Sun Y and Zhang H 2011 *ACS Nano* **6** 74
[66] Artola A, Kamal A, Ramakers G M J, Biessels G J and Gispen W H 2005 *J. Neurosci.* **22** 169

Supplementary Materials: Polymer-Decorated 2D MoS_2 Synaptic Transistors for Biological Bipolar Metaplasticities Emulation

Yuhang Zhao(赵宇航), Biao Liu(刘标), Junliang Yang(阳军亮),

Jun He*(何军), and Jie Jiang*(蒋杰)

Hunan Key Laboratory of Super Microstructure and Ultrafast Process, School of Physics and Electronics, Central South University, Changsha, Hunan 410083, China
Corresponding authors: Email: jiangjie@csu.edu.cn; junhe@csu.edu.cn

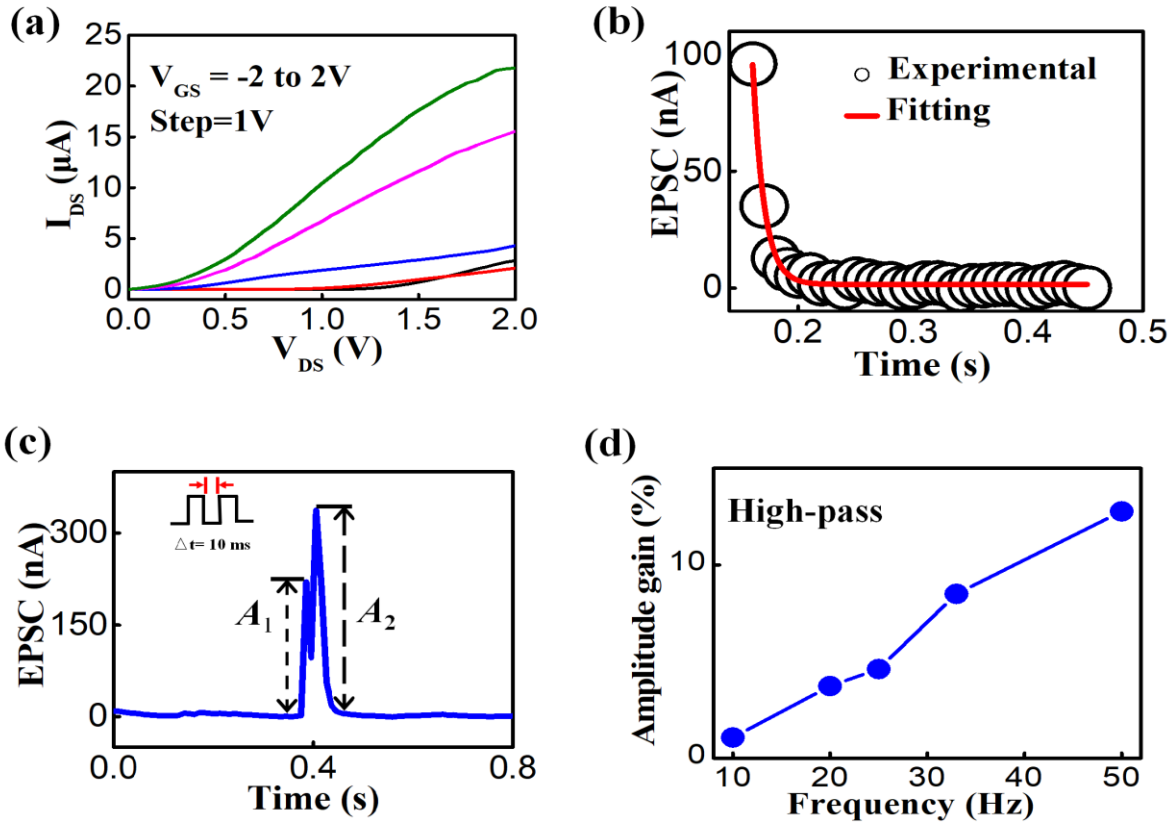

Fig. S1. (a) The output curve of PVA-decorated MoS_2 transistor by sweeping the V_{DS} from 0 V to 2 V with V_{GS} from -2 V to 2 V, with 1 V steps. (b) EPSC decay phenomenon by using the exponential decay model. (c) A pair of presynaptic spikes and a triggered EPSC are shown versus time. (d) EPSC amplitude ratio (A_{10}/A_1) plotted as a function of the presynaptic spike frequency.

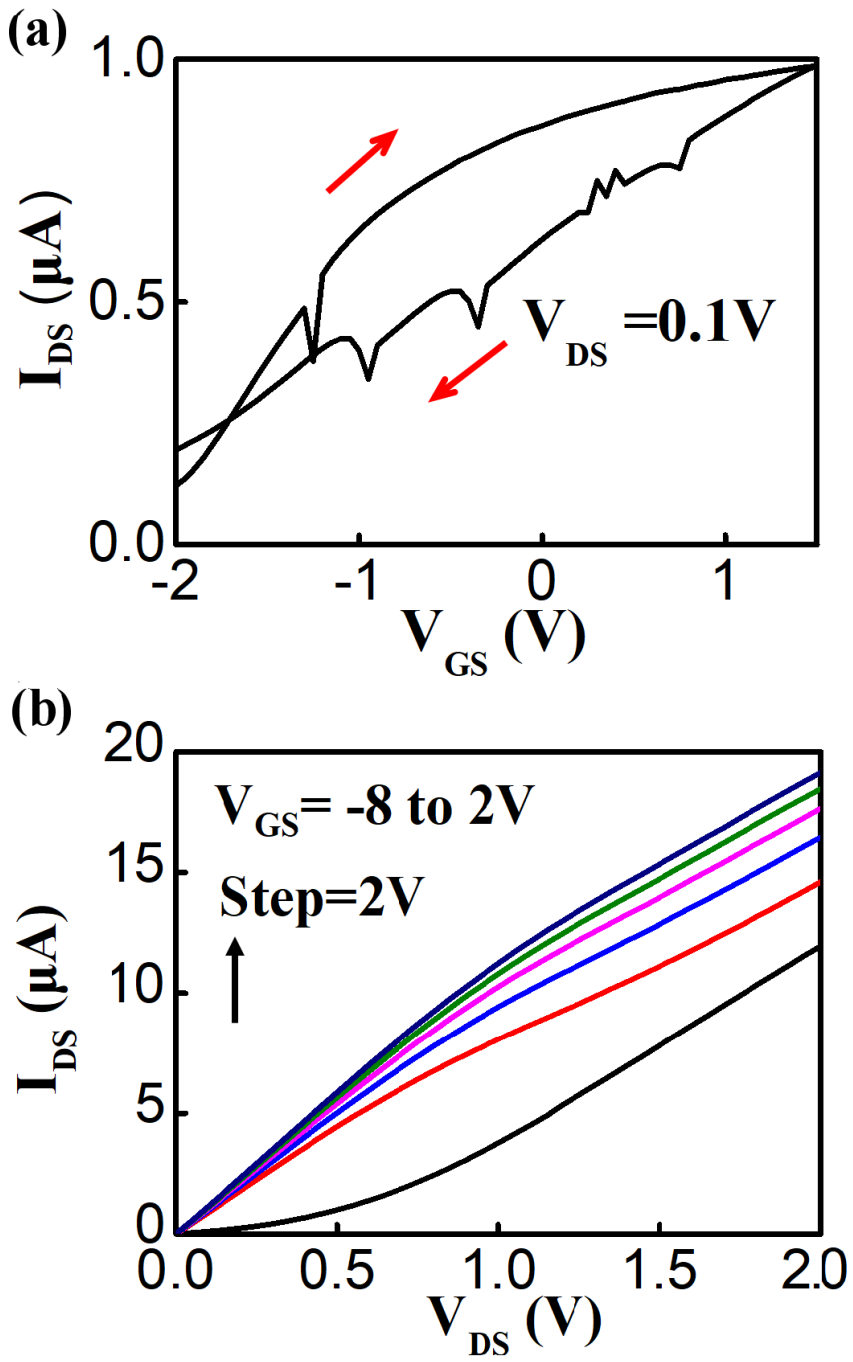

Fig. S2. (a) The transfer curve of the chitosan-decorated MoS_2 transistor with a fixed bias of V_{DS} = 0.1 V. (b) The output curve of chitosan-decorated MoS_2 transistor by sweeping the V_{DS} from 0 V to 2 V with V_{GS} from -8 V to 2 V with 2 V steps.

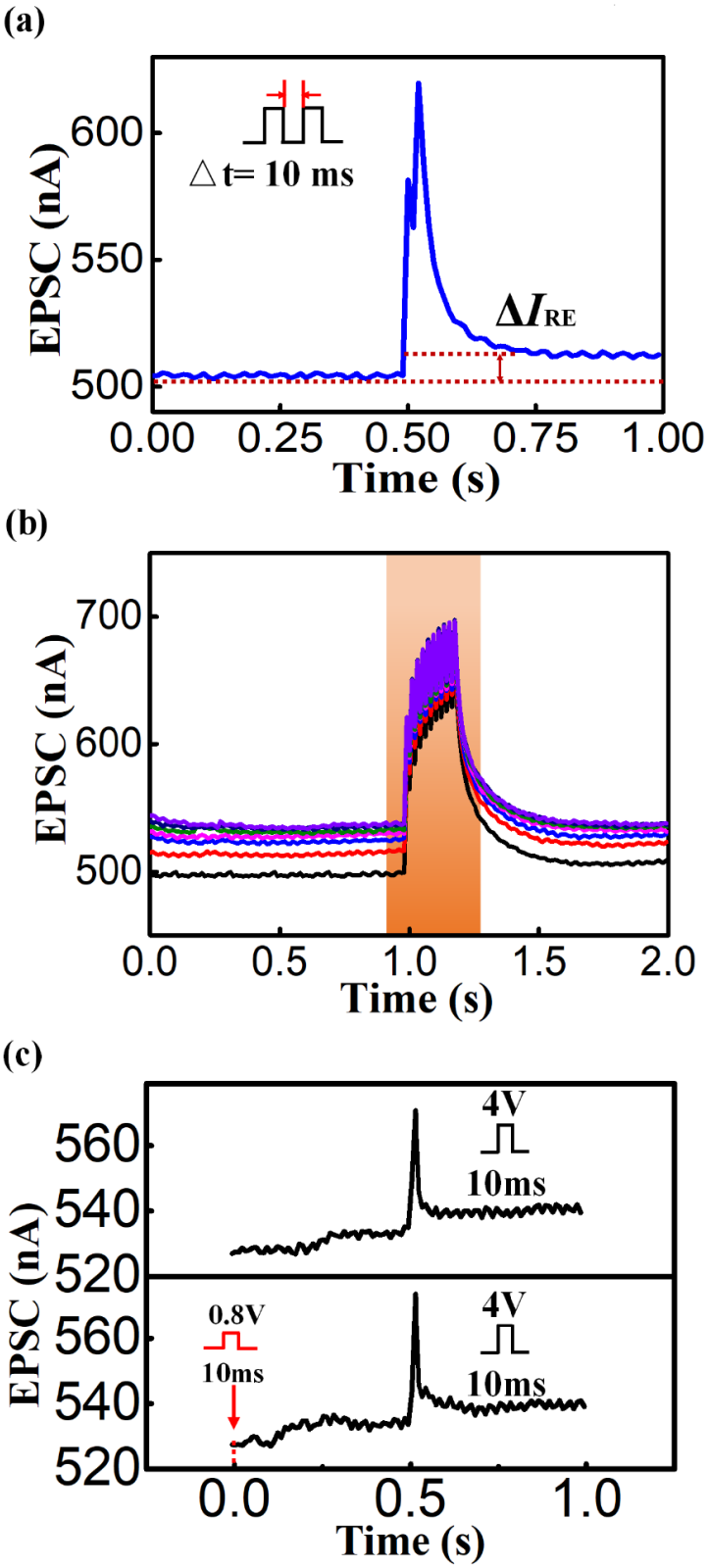

Fig. S3. (a) A pair of presynaptic spikes and a triggered EPSC are shown versus time. (b) The EPSCs triggered by the successive gate electric spikes with the same amplitudes (4 V, 10 ms) for seven times. (c) Typical metaplasticity of LTP phenomenon.

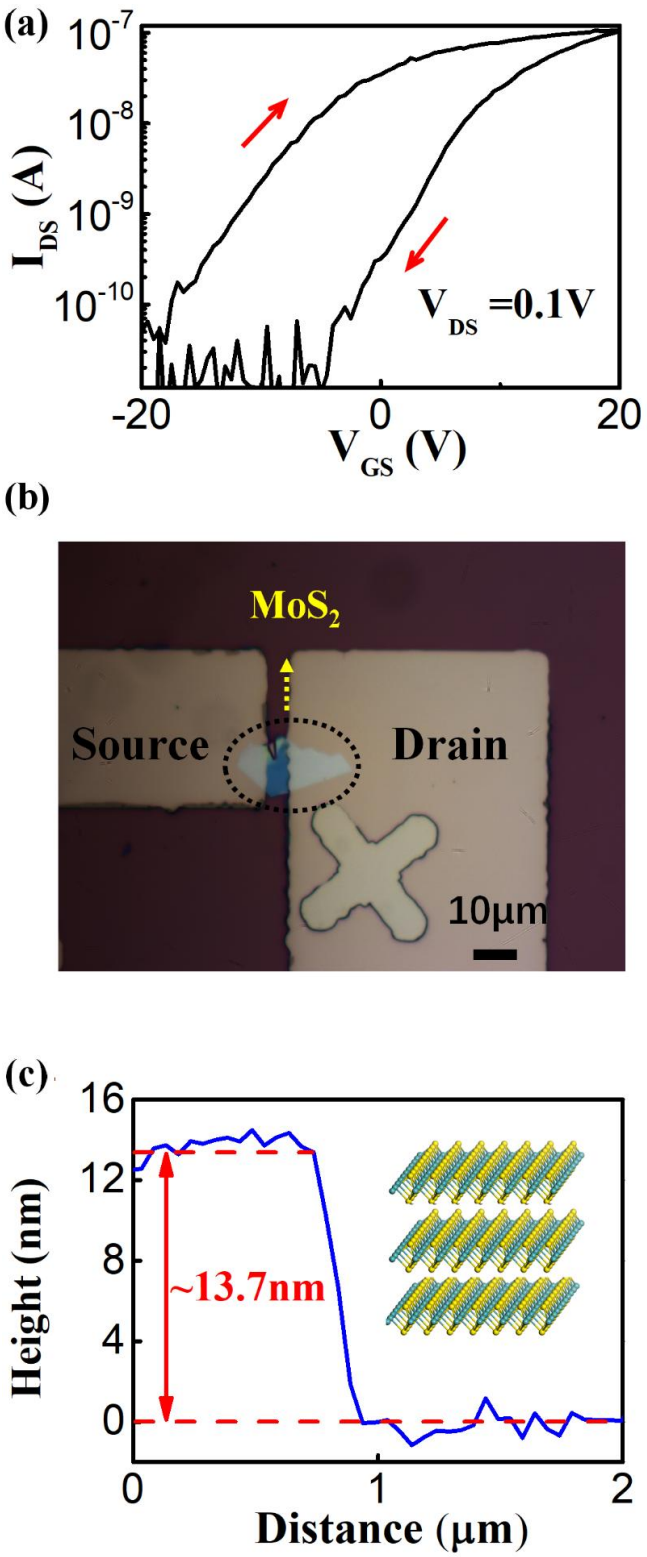

Fig. S4. (a) The transfer curve of the bottom-gate MoS_2 transistor with a fixed bias of V_{DS} = 0.1 V (without surface polymer decoration). (b) A top-view optical image of the device. (c) AFM measurement at the MoS_2 flake edge. Inset: schematic diagram of layered atomic structure of multilayer MoS_2.

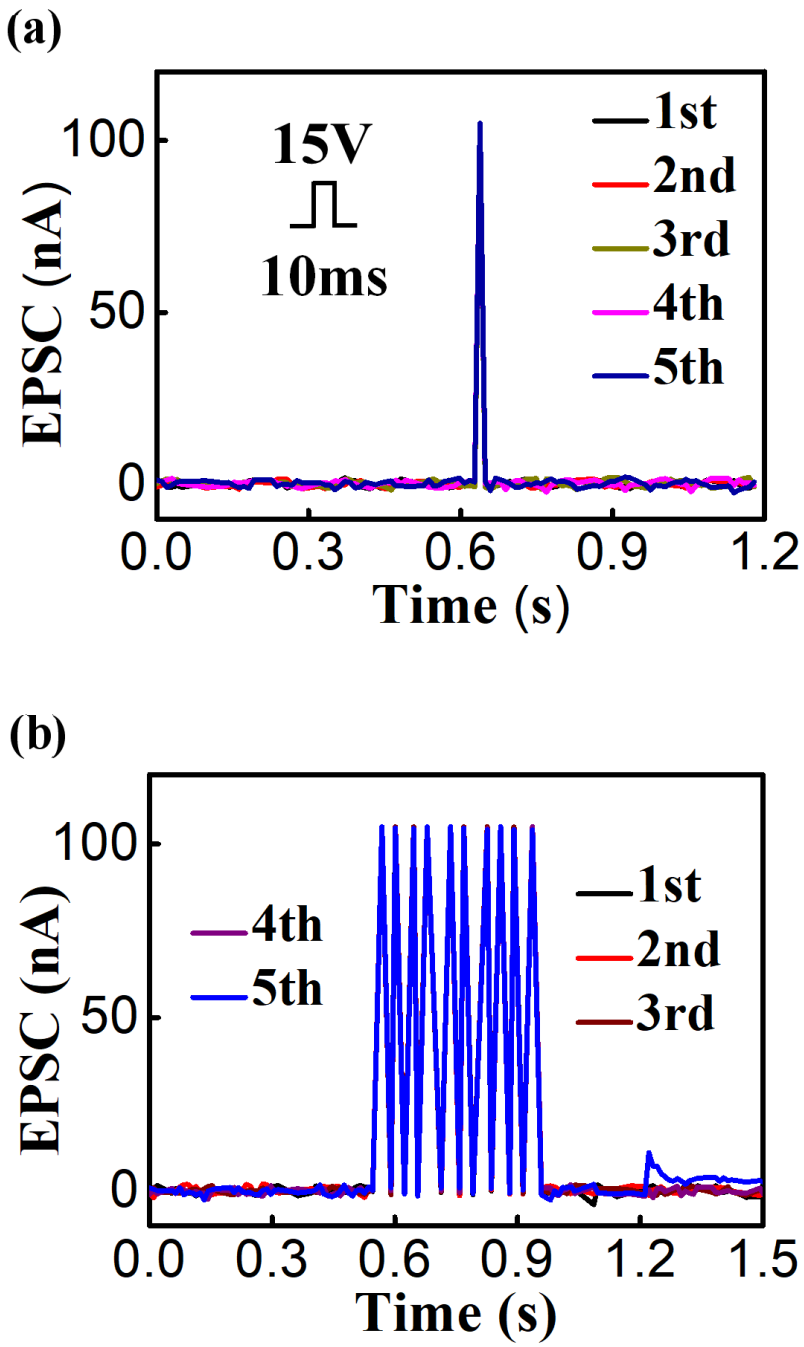

Fig. S5. (a) Five transient EPSC responses measured repeatedly under the same amplitudes of the gate electric spikes (15 V, 10 ms) (without surface polymer decoration). (b) The channel current responses triggered by the same amplitudes of the gate electric spikes (15 V, 10 ms) for five times.